Electronic properties of α-quartz under pressure

N. Binggeli, N. Troullier, José Luís Martins, and James R. Chelikowsky
Department of Chemical Engineering and Materials Science and Minnesota Supercomputer Institute, University of Minnesota, Minneapolis, Minnesota 55455
(Received 25 April 1991)

The electronic structure of α-quartz is investigated within the local-density formalism using recently developed *soft* pseudopotentials. We present results for the band structure, density of states, and charge density of α-quartz at ambient pressure and near the crystalline-to-amorphous transition. The results at ambient pressure compare well with experiment, and are generally consistent with earlier theoretical analysis. Pressure is found to induce a strong interaction between the Si—O bonding and O $2p$ lone-pair valence states. The gap between the corresponding bands vanishes in the region of the transition to the glass phase. The fundamental band gap increases, instead, with increasing pressure. Trends in the pressure dependence of the electronic structure are discussed in connection with the distortion of the oxygen sublattice towards an ideal close-packed configuration.

I. INTRODUCTION

From a technological point of view, silicon dioxide is one of the most useful wide-gap materials. SiO_2 plays a crucial role in silicon-based electronic devices, as well as in the glass and ceramic industry. From a geological point of view, silica is one of the main constituents of the Earth's crust and mantle, and the investigation of the pressure-induced structural transitions of SiO_2 and its high-pressure polymorphs is of fundamental interest.

Most common forms of silica, including α-quartz and high-pressure or high-temperature phases such as cristobalite, coesite, and tridymite, are composed of chains of the same fundamental structural unit, the SiO_4 tetrahedron. The O-Si-O angles, in these polymorphs at equilibrium, are close to the ideal tetrahedral bond angle of 109.5°. Oxygens are bound to two silicon atoms, and interconnect the silica tetrahedra. The way in which the tetrahedra are linked together (Si-O-Si angle) and form rings determine the overall symmetry of the crystals and differentiate the polymorphs. The properties of fourfold coordinated silica in crystalline and amorphous forms are very similar, and suggests a similarity of the bonding units and their environment.

The electronic properties of silica have been extensively discussed in the framework of semiempirical approaches.[1–3] On the other hand, most first-principles investigations of silica and silicate systems have been done on molecules or model clusters.[4–6] In particular, a number of Hartree-Fock calculations[7,8] have been performed to investigate the electronic charge density and bonding properties of molecules with Si—O bond angles and bond lengths that resemble those of silica crystals. The general goal of these studies was to improve our understanding of the properties of the Si—O bond and generate interatomic potentials to be used in computer simulation of SiO_2 structural phase transitions[6,9,10] or amorphous SiO_2.[11] There have been only a few self-consistent solid-state calculations of the electronic properties of SiO_2 polymorphs,[12–15] and only very recently the structural properties of these materials have also been evaluated from first principles.[16–19] To our knowledge, no self-consistent first-principles investigation of the pressure effects on the electronic structure of silica has been reported to date.

First-principles studies of the properties of SiO_2 polycrystals were impractical, until recently, because of the complexity of their crystalline structure. For complex systems, the pseudopotential approach significantly simplified the calculation of the electronic and structural properties. In the case of oxides, however, such calculations were hindered by the difficulty of handling oxygen ions within a pseudopotential plane-wave approach. The recent development of schemes to generate transferable pseudopotentials which are softer[20] and completely separable in momentum space,[21] as well as the development of more efficient computational techniques[22,23] using plane-wave basis, have made such calculations practical.

In this study, we focus on SiO_2 in the α-quartz structure. Among the various crystalline forms of silicon dioxide, α-quartz is the stable structure at room temperature and for pressures below 3 GPa. At higher pressures, α-quartz persists as a metastable form, and undergoes a gradual transition to an amorphous state at about 30 GPa.[24] There is some experimental evidence[24,25] that the onset of the transition may occur at somewhat lower pressure (15–25 GPa). The driving force for this unusual order-disorder transition is not well understood. It has been suggested that the transition might be associated with structural instabilities occurring when the oxygen atoms approach a close-packed configuration.[25] Experimental studies of α-quartz are presently limited to the investigation of pressure effects below the transition to the amorphous phase. First-principles theoretical investigations, on the other hand, have no such limitations. They offer the possibility to investigate phases which are difficult or impossible to study experimentally, such as α-quartz near and above the transition to the amorphous state. The structural properties of α-quartz under pressure have been described in a previous paper.[18] Here, we

concentrate on the electronic properties.

In Ref. 18, it was shown that the internal structural parameters of α-quartz evolve linearly up to 10–15 GPa, but have a highly nonlinear behavior above such pressure. The nonlinear behavior occurs near the onset of the transition to the amorphous phase, and could be interpreted as a change to highly strained geometries. To relieve such a strain, the crystal could transform to an amorphous structure. The interpolyhedral O-O distance and Si-O-Si angle, in particular, are considered key parameters which could trigger the unusual order-disorder transition. They both decrease linearly in the low-pressure regime, and then level off, when repulsion or strain effects become dominant. It was pointed out in Ref. 18, that the interpolyhedral O-O distance may play the key role, since this distance reaches a critical value[18] near the onset of the transition to the amorphous phase, while the Si-O-Si angle falls below the critical angle of 120° (where a sharp increase of the strain energy is suggested from molecular orbital calculations) only at much higher pressure. Because electronic structure and structural changes are intrinsically connected, the investigation of the changes in the electronic properties in the region where the order-disorder transition takes place may yield important information to understand the transition.

Another interesting issue of the pressure study concerns the properties of the α-quartz structure above the transition to the amorphous form. From an extrapolation of the trends observed during compression of α-quartz and its low-pressure isomorphic counterpart α-GeO_2, Sowa[26] suggested that the structure changes to a body-centered-cubic (bcc) packing of the oxygen ions. It was shown in Ref. 18 that some of the structural parameters were indeed relatively close to the value corresponding to the bcc packing. The c/a ratio, however, was found to be different from that expected for the bcc structure. The trends in the electronic properties may help in characterizing the important structural changes and assert the validity of Sowa's model for the high-pressure limit of the structural transformation.

This work is organized as follows: In Sec. II, we review briefly the calculation method. In Sec. III A, we examine the charge density, band structure, and density of states (DOS) of α-quartz at ambient pressure, and compare our results with the available experimental information and earlier theoretical results. In Sec. III B, we investigate the effect of pressure on the electronic properties below, near, and above the transition to the amorphous state. Trends in the pressure effects are also discussed in connection with the limit of a closed-packed bcc configuration of oxygen atoms.

II. CALCULATIONAL DETAILS

The calculations have been performed within the local-density approximation (LDA) of the density-functional theory, using the plane-wave pseudopotential method.[27] We used the exchange-correlation potential of Ceperley and Alder[28] as parametrized by Perdew and Zunger.[29] The details of the calculation have been described elsewhere,[18] and we review here only selected aspects.

The calculations are based on first-principles norm-conserving pseudopotentials generated with the method of Troullier and Martins.[20] This method produces soft pseudopotentials, which considerably reduce the number of plane waves needed to achieve convergence in the total-energy calculations. The oxygen pseudopotential was generated from the $2s^2 2p^4$ non-spin-polarized oxygen atomic valence ground-state configuration, using a core radius cutoff of 1.45 a.u. for both the s and p pseudopotential components. The nonlocal d component was neglected owing to the high energy of the d states relative to the $2s$ and $2p$ atomic valence states. For silicon s, p, and d components were generated from the $3s^2 3p^2 3d^0$ valence configuration of the non-spin-polarized atomic ground state. The cutoff radius used in this case was 1.8 a.u. for all three components.

The pseudopotentials were transformed into the computational efficient Kleinman-Bylander separable form,[21] using the p component as the local part for both the oxygen and silicon pseudopotentials. In general, the pseudopotential component with the highest angular momentum is chosen as the local part, and simulates the potential for states with higher angular momenta. In the case of silicon, however, the p component was selected as the local part, since it gave a total pseudopotential with a higher degree of transferability. The oxygen and silicon pseudopotentials used here in separable form both satisfy the criteria for absence of ghost states.[18] To reduce computational time and storage, the one-electron Schrödinger equations were solved using a fast iterative diagonalization technique in conjunction with the dual-space method.[22,23] Plane waves up to an energy cutoff of 64 Ry were included in the basis set, and one special **k** point was used in the total-energy calculations for the Brillouin-zone integrations.

The unit cell of α-quartz contains six oxygen and three silicon atoms. The structure has hexagonal D_3^4 symmetry, and is defined by the lattice constants (c,a) and four internal parameters (u,x,y,z). The parameter u and the set of parameters (x,y,z) define the Si and O ion positions in the unit cell, respectively. The ion coordinates are explicitly given in terms of these parameters in Ref. 18. The electronic structure has been evaluated self-consistently for different volumes Ω of the hexagonal unit cell. These volumes correspond to pressures running from zero to $\sim$60 GPa (we used the pressure-volume relation of Ref. 18). For each volume the calculations have been performed with completely relaxed structural parameters $(c/a,u,x,y,z)$. These parameters have been reported as a function of pressure in a previous article.[18]

III. RESULTS AND DISCUSSION

A. Electronic properties at zero pressure

In Fig. 1(a), we present the differential charge density, i.e., the difference between the crystal charge density, calculated for α-quartz at zero pressure, and the superposi-

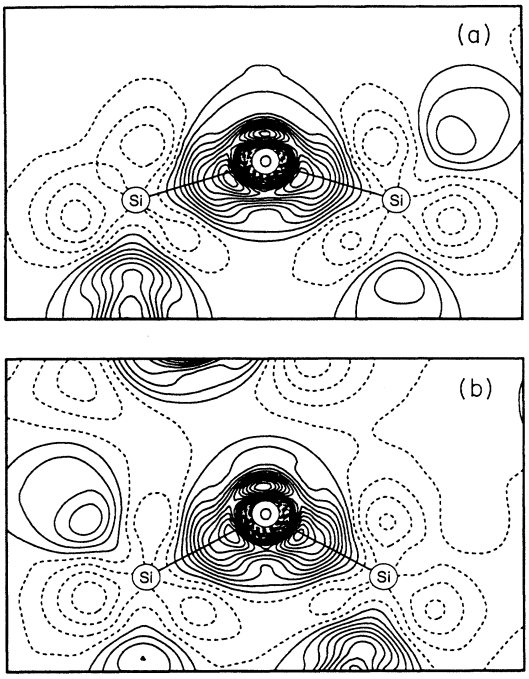

FIG. 1. Difference between the crystal charge density and the superposition of atomic charge densities in the Si-O-Si plane for α-quartz at zero [panel (a)] and 30 GPa [panel (b)] of hydrostatic pressure. The lines of equal density are separated by $5e/\Omega_0$. The dashed lines indicate regions where the electronic charge has decreased, the solid lines correspond to zero or positive densities.

tion of atomic charge densities. The charge is displayed in the Si—O—Si bonding plane. The contours of equal charge accumulation and charge depletion are indicated by solid and dashed lines, respectively. The bonding peaks in the density maps lie inside the Si-O-Si angle, near the lines joining the Si and O atoms, at a distance of ~0.50 Å (i.e., ~31% of the bond length) from the O atom. This indicates a relatively high ionicity in the oxide bond, and Fig. 1(a) shows that there is a significant charge transfer from the Si to the O atomic valence regions. The bonding charge comes in large part from regions along the bond axis, behind the Si atom, i.e., essentially from the Si atom valence charge located the furthest away from the oxygen. In a bonding-orbital picture, the depletion regions correspond to antibondinglike Si-O orbitals, exhibiting here dominant Si character. Charge accumulation also occurs outside the Si-O-Si angle, behind the O atom, and is associated with the O nonbonding orbitals. Based on Fig. 1(a), the Si–O bond can be characterized as a mix of covalent and strong ionic bonding, which coexist with O nonbonding features.

Our charge density difference in Fig. 1(a) shows strong similarities with the experimental deformation map of coesite,[8] in the four nonequivalent Si-O-Si planes with Si-O-Si angles between 137° and 150° (this angle is 144° in α-quartz). Similarities include the main features of the O—Si bonding charge in Fig. 1(a), i.e., the elongated shape of the bonding feature with a slow decrease of the density in the direction of the Si atom, the peak maximum situated slightly inside the Si-O-Si angle, and relatively close to the O atom, and finally the peak height [which is $\sim 0.45e$ Å^{-3} in Fig. 1(a), and between 0.4 and $0.49e$ Å^{-3} in Ref. 8]. The charge accumulation in the nonbonding region in Fig. 1(a) also appears in the deformation maps of Ref. 8 in the two planes with Si-O-Si angles of 138° and 150°. This feature is not observable in the two other planes with Si-O-Si angles of 143° and 144°, presumably because of the limited resolution of the data.[8]

In Fig. 2(a), we present the band structure of α-quartz along the high-symmetry directions of the hexagonal Brillouin zone. The zero of the energy scale corresponds to the valence band maximum. The material is an indirect gap insulator, with a 5.8-eV gap occurring between the valence maxima at K and M and the conduction band minimum at Γ. The difference between the valence band maximum at K and the extremum at M is only 0.02 eV, i.e., smaller than the accuracy of the present calculation. The other high-symmetry points correspond to maximum valence energy a few tenths of eV lower than the K and M points. The theoretical band gap significantly underestimates (35%) the experimental optical gap (8.9 eV), as expected from LDA ground-state calculations. The value of the band gap obtained here is consistent with the value of 5.6 eV obtained by Xu and Ching[15] from recent LDA calculations using the linear combination of atomic orbitals (LCAO) approach. In earlier studies the gap was either fitted to the experimental optical gap[2,3] or, in the case of the nonempirical pseudopotential calculations,[12] was found to be of the same magnitude, most likely because pseudopotentials with a lower degree of transferability and a more limited basis set were used in the earlier work.

The valence band structure at zero pressure consists of three groups of bands well separated in energy. In the three panels on the left-hand side of Fig. 3, we show separately the contributions from these sets of bands to the valence pseudocharge density. These charge densities are shown in the Si—O—Si bonding plane. The six lowest bands clearly consist of O $2s$ or semicore localized $3s$ states [panel (a)], the next six bands are predominantly composed of O $2p$–like and Si bonding states [panel (b)], while the upper 12 bands with low dispersion consist essentially of O $2p$–like nonbonding states [panel (c)]. The nature of the bonding states is consistent with the result of earlier theoretical investigation.[12] We note, however, that except for the charge density determined from Hartree-Fock calculations,[14] our densities show stronger ionic character than reported earlier.[12] We attribute this, again, to the difference in the pseudopotentials and energy cutoff; the larger cutoff used here allows a higher degree of charge localization.

In Fig. 4(a), we present the calculated DOS at zero pressure together with the x-ray photoemission spectroscopy (XPS) data reported in Ref. 2. Taking into account the fact that XPS measurements enhance features with s-like character—in particular the low-energy region of the O $2p$–Si sp^3 hybrid bonding band—the calculated DOS structure for the two upper valence bands agrees ex-

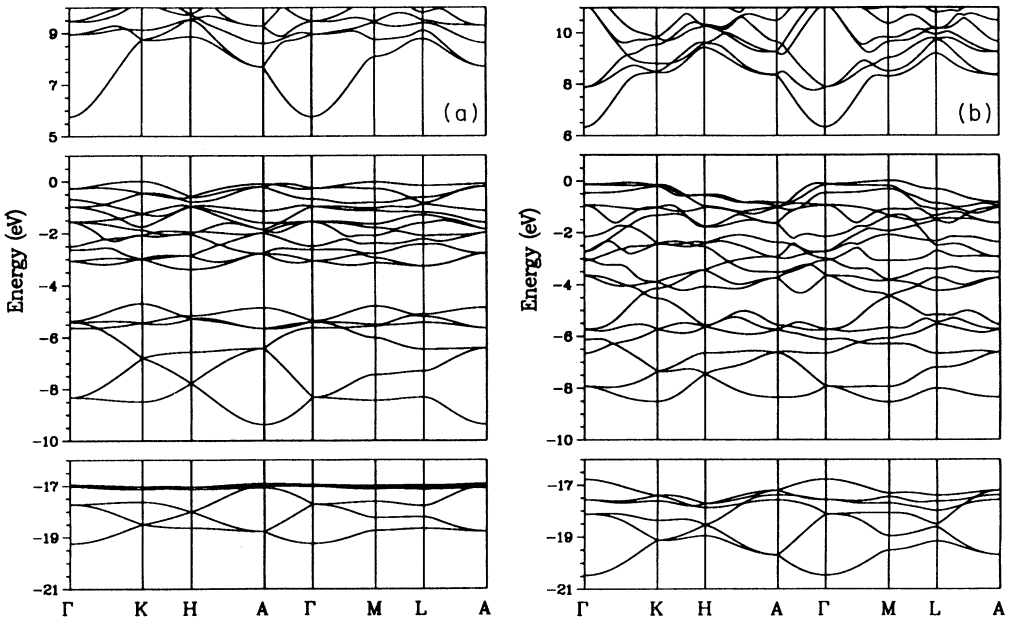

FIG. 2. Band structure of α-quartz at zero (a) and 30 GPa (b).

tremely well with experiment. The XPS O 2s peak, instead, is located between $\sim$20 eV (Ref. 30) and 21 eV (Ref. 31) below the valence band edge, while the corresponding DOS peak in Fig. 4(a) is only $\sim$18 eV below the valence band maximum. The O 2s states, however, essentially behave as core states, and it is well known that the difference in the energy position of core and valence XPS features is several eV larger than the difference between the corresponding one-electron energy levels, because of the electron-hole interaction.

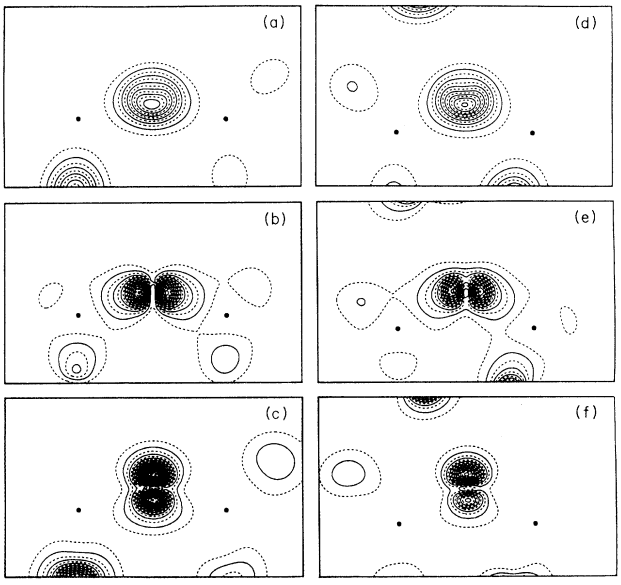

FIG. 3. Pseudocharge density of the three characteristic groups of valence bands for α-quartz at zero (left panels) and 30 GPa (right panels). The charge densities are displayed in the Si—O—Si bonding plane. The positions of the Si atoms are indicated by dots. The lines of equal density are separated by $20e/\Omega_0$.

Comparing our results with other calculations, we find very good quantitative agreement with the band structure obtained recently by Xu and Ching[15] from self-consistent LCAO calculations. Our band structure and valence DOS are also in overall agreement with earlier calculations,[2,3,12–14] although some noticeable differences exist in the valence band widths and band positions. The width of the upper two valence bands is 1–2 eV larger than predicted by the non-self-consistent LCAO calculation in Ref. 3. Earlier self-consistent calculations using pseudopotential[12] or mixed basis[13] approaches with a more limited basis set, or using the Hartree-Fock approach[14] predict, instead, bandwidths 1–2 eV larger than the present results. The position of the O 2s band relative to the valence band edge is also 6 eV lower in Ref. 12, and the O 2s bandwidth 1 eV smaller, than in the present study. We note that using a lower-energy cutoff (18 Ry), more similar to that used in Ref. 12, we also obtain a larger separation between the upper valence and the O 2s bands ($\sim$24 eV), a smaller O 2s bandwidth ($\sim$1 eV), and a larger bandwidth for the upper valence band ($\sim$4 eV). The location of the valence band maximum in our results (K and/or M) differs from those predicted by several earlier band calculations,[2,13] which located the band edge at Γ or A. We also note that the onset of the DOS for the lowest empty states, in Fig. 4(a), is much more abrupt than in earlier theoretical studies,[2,3] and in better agreement with the result of inverse XPS measurements on amorphous SiO_2.[32] The photoemission data[2] for the valence bands of α-quartz and amorphous SiO_2 are essentially identical, except for fine structure, such as the three

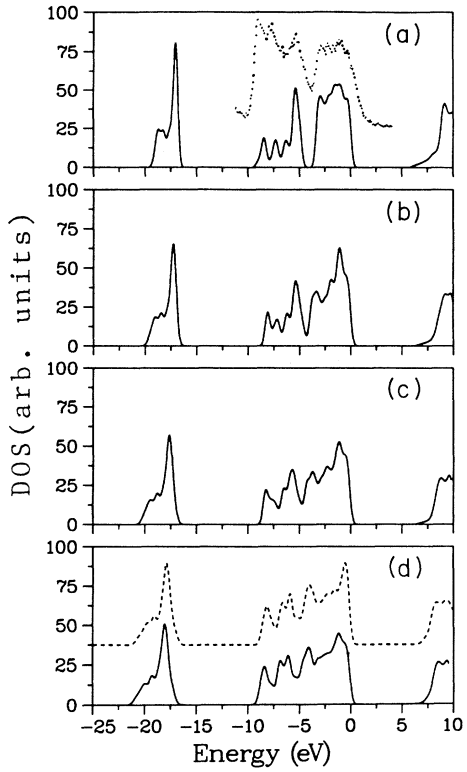

FIG. 4. Calculated density of states for α-quartz (full line) at zero [panel (a)], 17 [panel (b)], 30 [panel (c)], and $\sim$60 GPa [panel (d)]. In panel (a), we also show (dotted line) the XPS spectrum taken from Ref. 2 for the upper two valence bands, and in panel (d), the density of states (dashed line) calculated for the limiting case of a close-packed body-centered-cubic structure of oxygen ions (Ref. 26) (the volume is the same as calculated at 60 GPa, i.e., $\Omega/\Omega_0=0.65$, and we use the optimized silicon u parameter 0.4103). The theoretical results have been convoluted with a Gaussian broadening function of full width at half maximum of 0.5 eV.

peaks at the bottom of the valence O $2p$–Si bonding band [see the DOS in Fig. 4(a)], which can be associated with long-range order in α-quartz.[2] Generally similar features are also expected for the empty states spectra of the two materials.[2]

B. Pressure effects

We examine here the electronic properties of α-quartz in the region where the gradual pressure-induced transition to the glass phase occurs. The features of this transition and the properties of α-quartz near and above the transition are not clear at present.

The differential charge density in the Si—O—Si bonding plane at zero and 30 GPa ($\Omega/\Omega_0=0.72$) are displayed in Figs. 1(a) and 1(b), respectively. The Si-O-Si angles are $\sim$144° and $\sim$120° in Figs. 1(a) and 1(b), respectively. The major changes in the electronic density associated with the large bond bending in Fig. 1(b) are the distortion of the O nonbonding feature towards the bonding peak on the left-hand side of the figure, and the charge transfer from this peak to the bonding peak on the right-hand side and to the nonbonding peak. Pressure also induces a shallow negative valley of charge density between the Si atoms with a small density bridge between neighboring oxygen ions [center and top center section of Fig. 1(b)], which occurs when the O atoms are brought relatively close to each other. The remaining changes, in this plane, such as the reversal of the environment of the left- and right-most Si atoms, simply reflect the lattice distortion.

The band structure at 30 GPa is displayed in Fig. 2(b). Under moderate hydrostatic pressure the band gap increases, and is found equal to 6.4 eV at 30 GPa, with the valence band maximum at the M point. The gap increase is linear below $\sim$5 GPa, and the pressure coefficients $\partial E_g/\partial p$ for the K^v-Γ^c, M^v-Γ^c, and Γ^v-Γ^c gaps are $\sim$9, 10, and 7 meV/kbar, respectively. At pressure larger than 10 GPa, the gap has a highly nonlinear behavior, as expected since the internal parameters also behave nonlinearly in this region. The gap slightly decreases ($\sim$0.1 eV) near 20 GPa, and increases again at higher pressure. We note that the energy of the lowest conduction state at K, in particular, decreases with pressure relative to the valence band maximum. By applying sufficient pressure, one can imagine that the conduction band minimum will eventually change from the Γ to the K point. This, however, may happen only at much higher pressures than those considered here (above the limit where the pseudopotential calculation loses its validity because of core overlapping).

A striking change in Fig. 2(b) is the disappearance of the gap between the O—Si bonding bands and the O nonbonding bands. Important anticrossing features and repulsion features (e.g., at Γ) appear between these two sets of bands in Fig. 2(b), indicating that strong hybridization takes place between the bonding and nonbonding states [see Figs. 5(f) and 5(g)]. The partial charge density associated with these two sets of bands and the O $2s$ corelike band at 30 GPa are shown in the Si—O—Si bonding plane in the right-most panels of Fig. 3. There is a relatively strong distortion of the O p–like orbitals in Figs. 3(e) and 3(f). The bonding orbitals in Fig. 3(e) tend to bend towards the neighboring Si ions, following the bending of the Si-O-Si angle. Bridges of charge density appear between neighboring O ions, resulting in a stronger asymmetry of the O–Si bonding features. The nonbonding orbitals in Fig. 3(f) become also more asymmetric. There is a noticeable compression of the charge outside the Si-O-Si angle, and a small anticlockwise rotation of the feature in Fig. 3(f), which account for the distortion of the nonbonding peak in the differential density map [Fig. 1(b)].

General trends in the effect of pressure on the DOS are clearly seen in Fig. 4, when comparing results at zero pressure (a), 17 GPa, ($\Omega/\Omega_0=0.84$) (b), 30 GPa (c), and $\sim$60 GPa ($\Omega/\Omega_0=0.65$) (d). The two upper valence bands merge in a single DOS structure with four dominant features. Such features are associated with characteristic individual charge densities. In Fig. 5 (right-most

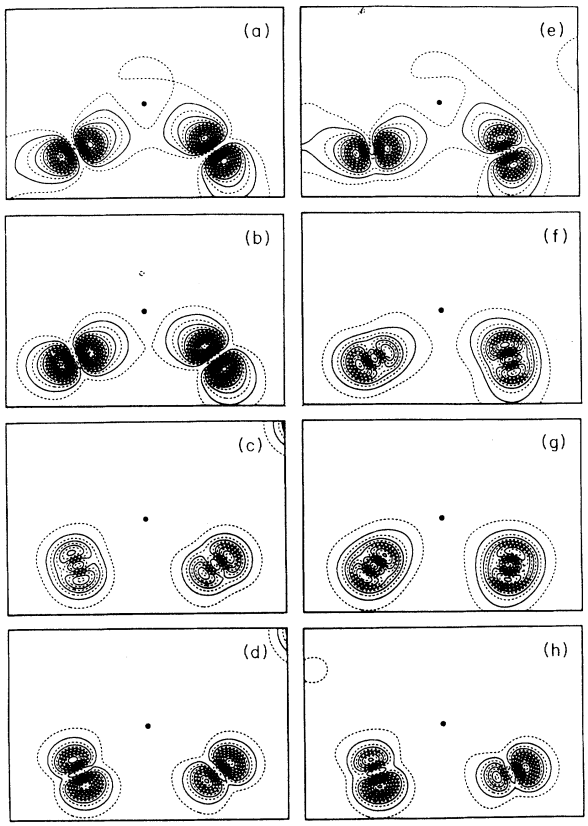

FIG. 5. Pseudocharge density of the four sets of bands which give rise to the main features in the density of states at high pressure. The panels on the right-hand side show the densities at 30 GPa, while the panels on the left-hand side show the densities for the same groups of bands at zero pressure. The densities are displayed in the O—Si—O bonding plane, and the lines of equal density are separated by $10e/\Omega_0$ in panels (a)–(c) and (e)–(g), and $30e/\Omega_0$ in panels (d) and (h).

panels), we show the 30 GPa charge density in the O—Si—O bonding plane associated with each individual peak. In the left-most panels, we show for comparison the corresponding partial charge densities at zero pressure. The nature of the states corresponding to the two DOS peaks with the lowest and highest energy [Figs. 5(e) and 5(h), respectively] are not significantly altered. They essentially remain the strongly bonding O $2p$–Si sp^3 and O $2p$ lone-pair states found at the bottom of the lowest and top of the highest upper two valence bands of α-quartz at zero pressure [Figs. 5(a) and 5(d), respectively]. The other two DOS peaks, instead, are associated with strongly hybridized bonding and nonbonding states. The density associated with the second peak becomes increasingly spherical [see Fig. 5(f) as compared to Fig. 5(b)], and for the third peak, we see that the orbitals associated with the O atom on the left-hand side of Fig. 5 change from non-bonding-like features at zero pressure [Fig. 5(c)] to almost bondinglike features at 30 GPa [Fig. 5(g)]. These important changes result in the distortion of the nonbonding feature and charge transfer between the different density peaks noticed in the density map in Fig. 1(b).

The pressure evolution of the DOS tends towards the four-peak structure in Fig. 4(d), which was obtained for a compression $\Omega/\Omega_0=0.65$ corresponding to the transformation of the oxygen sublattice in a close-packed configuration [Fig. 1 of Ref. 33], with structural parameters[18] $x\approx\frac{1}{3}$, $y\approx\frac{1}{3}$, $z\approx\frac{1}{12}$. The oxygen lattice geometry $(c/a,x,y,z)$ remains essentially constant at lower volumes (we examined compression as large as $\Omega/\Omega_0=0.5$). With the structural parameters $x=\frac{1}{3}$, $y=\frac{1}{3}$, $z=\frac{1}{12}$, and $c/a=\sqrt{\frac{3}{2}}\approx1.22$ (this ratio changes from 1.12 at zero pressure to 1.15 at $\sim$60 GPa), the oxygens form a close-packed configuration of bcc Wigner cells. This is the structure proposed by Sowa[26] as the high-pressure form of α-quartz. The DOS associated with this model limiting case of the oxygen ion packing, is also shown (dashed line) in Fig. 5(d). The characteristic features found for the ideal bcc oxygen lattice are essentially the same as obtained for the structure at $\sim$60 GPa. Although the c/a ratio is somewhat different at 60 GPa and in Sowa's model bcc structure, with respect to the *electronic* properties, Sowa's configuration can indeed be considered as the limit of the high-pressure evolution of the α-quartz structure.

IV. CONCLUSIONS

We have investigated the electronic properties of α-quartz using a first-principles approach. The pressure dependence of the electronic structure has been investigated below and above the crystalline-to-amorphous transition. The results at ambient pressure show good agreement with experiment. Important changes occur in the electronic structure as a result of increasing pressure. The energy gap between the O $2p$–Si bonding bands and the O $2p$ nonbonding band vanishes at about 30 GPa. The fundamental gap increases, instead, with increasing pressure. At 30 GPa, both the large Si—O—Si bond bending, and the small O-O distance are associated with important distortion in the bonding charge. Strong hybridization occurs between O—Si bonding and O nonbonding states, which gives rise to distinct features in the density of states. The trends in the calculated pressure effects show that for the electronic properties, the oxygen close-packed bcc configuration proposed by Sowa can be considered as the high-pressure limit of the evolution of the α-quartz structure.

ACKNOWLEDGMENTS

This work was supported by the Department of Energy under Grant No. DE-FG02-89ER45391, and by the Minnesota Supercomputer Institute. One of us (N.B) acknowledges support from the Swiss National Science Foundation. We also wish to acknowledge helpful conversations with Dr. H. E. King, Jr.

[1]S. T. Pantelides and W. A. Harrison, Phys. Rev. B **13**, 2667 (1976).
[2]R. B. Laughlin, J. D. Joannopoulos, and D. J. Chadi, Phys. Rev. B **20**, 5228 (1979); the α-quartz photoemission spectrum presented in this article was provided by R. Pollak.
[3]Y. P. Li and W. Y. Ching, Phys. Rev. B **31**, 2172 (1985), and references therein; I. Stich, Solid State Commun. **58**, 705 (1986).
[4]A. C. Lasaga and G. V. Gibbs, Phys. Chem. Minerals **14**, 107 (1987), and references therein.
[5]G. J. Kramer, N. P. Farragher, B. W. H. van Beest, and R. A. van Santen, Phys. Rev. B **43**, 5068 (1991); B. W. H. van Beest, G. J. Kramer, and R. A. van Santen, Phys. Rev. Lett. **64**, 1955 (1990).
[6]S. Tsuneyuki, M. Tsukada, H. Aoki, and Y. Matsui, Phys. Rev. Lett. **61**, 869 (1988).
[7]See, e.g., M. O'Keeffe and G. V. Gibbs, J. Phys. Chem. **89**, 4574 (1985).
[8]K. L. Geisinger, M. A. Spackman, and G. V. Gibbs, J. Phys. Chem. **91**, 3237 (1987).
[9]S. Tsuneyuki, Y. Matsui, H. Aoki, and M. Tsukada, Nature **339**, 209 (1989).
[10]S. Tsuneyuki, H. Aoki, M. Tsukada, and Y. Matsui, Phys. Rev. Lett. **64**, 776 (1990).
[11]L. V. Woodcock, C. A. Angell, and P. Cheeseman, J. Chem. Phys. **65**, 1565 (1976).
[12]J. R. Chelikowsky and M. Schlüter, Phys. Rev. B **15**, 4020 (1977).
[13]E. Calabrese and W. B. Fowler, Phys. Rev. B **18**, 2888 (1978).
[14]R. Dovesi, C. Pisani, C. Roetti, and B. Silvi, J. Chem. Phys. **86**, 6967 (1987).
[15]Y. Xu, and W. Y. Ching, *SiO_2 and its Interfaces,* edited by S. T. Pantelides and G. Lucovsky (MRS, Pittsburgh, PA 1988); Y. Xu, and W. Y. Ching, Physica B **150**, 32 (1988).
[16]D. C. Allan and M. P. Teter, Phys. Rev. Lett. **59**, 1136 (1987); J. Am. Ceram. Soc. **73**, 3247 (1990).
[17]K. T. Park, K. Terakura, and Y. Matsui, Nature **336**, 670 (1988), and references therein.
[18]J. R. Chelikowsky, H. E. King, Jr., N. Troullier, J. L. Martins, and J. Glinnemann, Phys. Rev. Lett. **65**, 3312 (1990); J. R. Chelikowsky, N. Troullier, J. L. Martins, and H. King, Jr., Phys. Rev. B **44**, 489 (1991).
[19]N. K. Keskar, N. Troullier, J. L. Martins, and J. R. Chelikowsky, Phys. Rev. **44**, 4081 (1991).
[20]N. Troullier and J. L. Martins, Solid State Commun. **74**, 613 (1990); Phys. Rev. B **43**, 1993 (1991).
[21]L. Kleinman and D. M. Bylander, Phys. Rev. Lett. **48**, 1425 (1982).
[22]J. L. Martins and M. L. Cohen, Phys. Rev. B **37**, 6134 (1988).
[23]N. Troullier and J. L. Martins, Phys. Rev. B **43**, 8861 (1991).
[24]R. J. Hemley, A. P. Jepcoat, H. K. Mao, L. C. Ming, and M. H. Manghnani, Nature **334** (1988).
[25]R. M. Hazen, L. W. Finger, R. J. Hemley, and H. K. Mao, Solid State Commun. **72**, 507 (1989).
[26]H. Sowa, Z. Kristallogr. **184**, 257 (1988).
[27]J. Ihm, A. Zunger, and M. L. Cohen, J. Phys. C **12**, 4409 (1979); **13**, 3095 (1980).
[28]D. M. Ceperley and B. J. Alder, Phys. Rev. Lett. **45**, 566 (1980).
[29]J. P. Perdew and A. Zunger, Phys. Rev. B **23**, 5048 (1981).
[30]T. H. DiStefano and D. E. Eastman, Phys. Rev. Lett. **27**, 1560 (1971).
[31]H. Ibach and J. E. Rowe, Phys. Rev. B **10**, 710 (1974).
[32]M. Azizan, R. Baptist, A. Brenac, G. Cauvet, and T. A. Nguyen Tan, J. Phys. (Paris) **48**, 81 (1987).
[33]N. Binggeli and J. R. Chelikowsky, Nature (to be published).